# Intercomparison of Atmospheric GCM Simulated Anomalies Associated with the 1997/98 El Niño

I.-S. KANG,[a] K. JIN,[a] K.-M. LAU,[b] J. SHUKLA,[c] V. KRISHNAMURTHY,[c] S. D. SCHUBERT,[d] D. E. WALISER,[e] W. F. STERN,[f] V. SATYAN,[g] A. KITOH,[h] G. A. MEEHL,[i] M. KANAMITSU,[j] V. YA. GALIN,[k] AKIMASA SUMI,[l] G. WU,[m] Y. LIU,[m] AND J.-K. KIM[a]

[a]*School of Earth and Environmental Sciences, Seoul National University, Seoul, Korea*
[b]*Climate and Radiation Branch, NASA GSFC, Greenbelt, Maryland*
[c]*Center for Ocean–Land–Atmosphere Studies, Institute of Global Environment and Society, Inc., Calverton, Maryland*
[d]*Data Assimilation Office, NASA GSFC, Greenbelt, Maryland*
[e]*Institute for Terrestrial and Planetary Atmospheres, State University of New York at Stony Brook, Stony Brook, New York*
[f]*NOAA/Geophysical Fluid Dynamics Laboratory, Princeton University, Princeton, New Jersey*
[g]*Indian Institute of Tropical Meteorology, Pune, India*
[h]*Meteorological Research Institute, Tsukuba, Ibaraki, Japan*
[i]*National Center for Atmospheric Research, Boulder, Colorado*
[j]*National Centers for Environmental Prediction, Camp Springs, Maryland*
[k]*Institute of Numerical Mathematics of Russian Academy of Sciences, Moscow, Russia*
[l]*Center for Climate System Research, University of Tokyo, Tokyo, Japan*
[m]*Institute of Atmospheric Physics, Beijing, People's Republic of China*

(Manuscript received 1 March 2001, in final form 11 December 2001)

ABSTRACT

The atmospheric anomalies for the 1997/98 El Niño–Southern Oscillation (ENSO) period have been analyzed and intercompared using the data simulated by the atmospheric general circulation models (GCMs) of 11 groups participating in the Monsoon GCM Intercomparison Project initiated by the Climate Variability and Prediction Program (CLIVAR)/Asian–Australian Monsoon Panel. Each participating GCM group performed a set of 10 ensemble simulations for 1 September 1996–31 August 1998 using the same sea surface temperature (SST) conditions but with different initial conditions. The present study presents an overview of the intercomparison project and the results of an intercomparison of the global atmospheric anomalies during the 1997/98 El Niño period. Particularly, the focus is on the tropical precipitation anomalies over the monsoon–ENSO region and the upper-tropospheric circulation anomalies in the Pacific–North American (PNA) region.

The simulated precipitation anomalies show that all of the models simulate the spatial pattern of the observed anomalies reasonably well in the tropical central Pacific, although there are large differences in the amplitudes. However, most of the models have difficulty in simulating the negative anomalies over the Maritime Continent during El Niño. The 200-hPa geopotential anomalies over the PNA region are reasonably well reproduced by most of the models. But, the models generally underestimate the amplitude of the PNA pattern. These weak amplitudes are related to the weak precipitation anomalies in the tropical Pacific. The tropical precipitation anomalies are found to be closely related to the SST anomalies not only during the El Niño seasons but also during the normal seasons that are typified by weak SST anomalies in the tropical Pacific. In particular, the pattern correlation values of the 11-model composite of the precipitation anomalies with the observed counterparts for the normal seasons are near 0.5 for the tropical region between 30°S and 30°N.

## 1. Introduction

The 1997/98 El Niño had a record-breaking intensity of sea surface temperature (SST) anomalies in the tropical Pacific and a profound impact on the global climate (Bell et al. 1999). A number of general circulation model (GCM) studies and GCM intercomparisons have been performed for previous El Niño events after 1980 (Blackmon et al. 1983; Lau 1985; Palmer and Mansfield 1986; Shukla and Fennessy 1988). In particular, the Atmospheric Model Intercomparion Project (AMIP) has provided a comprehensive evaluation of the performance of atmospheric GCM anomalies and has proven to be a useful reference of model sensitivity and predictability experiments to SST forcing (Gates et al. 1999; Boyle 1998). However, the AMIP experiment is limited to the period of 1979/96. Until now, a comprehensive GCM study using a group of GCMs has not been carried out for the 1997/98 El Niño.

Under this situation, by a request of the Climate Var-

*Corresponding author address:* Prof. In-Sik Kang, School of Earth and Environmental Sciences, Seoul National University, Kwanak-gu, Seoul 151-742, Korea.
E-mail: kang@climate.snu.ac.kr

iability and Prediction Program (CLIVAR) Science Steering Group, the present intercomparison project was initiated by the CLIVAR/Asian–Australian Monsoon Panel to evaluate a number of current atmospheric GCMs in simulating the global climate anomalies associated with the recent El Niño. The primary subjects of interest in the intercomparison project are the global ENSO and monsoon anomalies associated with the 1997/98 El Niño, the associated surface fluxes, and the intraseasonal oscillations. In the present study, as the first part of a series of reports of the intercomparison project, we focus on the global ENSO anomalies during the 1997/98 period, particularly the tropical rainfall anomalies and the upper-tropospheric circulation anomalies in the Pacific–North American (PNA) region.

The present intercomparison is similar to the AMIP except that the simulation period is September 1996–August 1998. Therefore, this experiment examines the atmospheric GCM responses to a given SST forcing over the globe. Given the primacy of tropical SST anomalies in forcing the global circulation anomalies (Lau and Nath 1994; Graham et al. 1994), it is anticipated that the present GCM results are dominated by the models' responses to tropical SST anomalies, particularly for the 1997/98 El Niño period. The quality of the GCM responses investigated in this study compared to the observations has implications for the ability of present GCMs to predict global climate anomalies for a given El Niño condition. In this regard, it is of interest to know the spread of various model responses to the SST specification compared to observations. But, this paper does not concentrate on the simulation of specific events or processes, nor does it emphasize the results of individual models here. Rather, the focus is on the performance of the models as a whole and seeking to summarize the systematic errors that are common to the current atmospheric GCMs.

Section 2 describes the experimental design of the present intercomparison project, the participating GCMs, and the observational data utilized. Section 3 provides an intercomparison of the precipitation anomalies simulated by the various models with particular attention paid to the tropical anomalies over the Pacific and the Asian monsoon region during the 1997/98 ENSO period. Section 4 discusses the model responses of upper-tropospheric circulation over the globe to the SST anomalies, and in particular, the ability of GCMs to reproduce the observed circulation anomalies over the PNA region during the 1997–98 winter, a mature phase of El Niño. Summary and concluding remarks are given in section 5.

## 2. Experimental design and data

For the present intercomparison, all participating GCM groups have performed a set of 10 ensemble experiments from the period 1 September 1996–31 August 1998 with the same SST boundary condition but with different initial conditions. The SST data used in these experiments are the observed pentad means from the Global Sea Ice and Sea Surface Temperature (GISST) dataset (Rayner et al. 1996) created by the Hadley Centre for Climate Prediction for the period January 1979–October 1981 and the Optimum Interpolation Sea Surface Temperature (OISST) analyses dataset (Reynolds and Smith 1994) created by the Climate Prediction Center (CPC) of the National Centers for Environmental Prediction (NCEP) for the period November 1981–December 1998. Because of the unavailability of the data for recent years, the sea ice is prescribed by the climatological monthly mean data utilized by the AMIP. Eleven modeling groups (COLA, DNM, GEOS, GFDL, IAP, IITM, MRI, NCAR, NECP, SNU, and SUNY/GLA) from six countries have provided experimental data to the coordinating institute, Climate Environment System Research Center at Seoul National University, Korea. The names of the participating institutes and their model descriptions are given in Table 1.

In addition to a set of ensemble simulations for the 1996–98 period, each GCM group performed an AMIP-type simulation, a 20-yr run with the observed SST from 1 January 1979 to 31 December 1998, to determine the model's climatological cycle. The SST anomalies of each model for the 1996–98 period are obtained by subtracting the 20-yr mean climatological cycle from the 2-yr simulation of the corresponding model. The only exception is the GEOS model climatology, which is for the shorter period of 1980–92, and all comparisons for this model with observations use the 1980–92 climatology. Although the spatial resolution of the models varies from rhomboidal truncation at wavenumber 15 to triangular truncation at wavenumber 42, all GCM data were converted to monthly averages and a spatial resolution of $2.5^\circ \times 2.5^\circ$ using a linear interpolation method. Note that the regridding algorithm conserves area mean quantities and does not affect the main results of the paper. The variables used here are precipitation for investigating tropical rainfall anomalies associated with the El Niño and geopotential height at 200 hPa for considering the upper-tropospheric circulation anomalies, especially over the Pacific/North American region.

The SST anomalies prescribed in the GCM experiment for the 2-yr period of 1996–98 are characterized by an evolution of a strong El Niño episode from the initiation to the termination. Therefore, they can be represented by the Niño-3.4 index, defined as the average of SST anomalies over the region of 5°S–5°N and 120°–170°W (Trenberth 1997). The time evolution of the Niño-3.4 index, shown in Fig. 1a, consists of a normal winter (December 1996–February 1997), a rather strong El Niño summer (June–August 1997), a strong El Niño winter (December 1997–February 1998), and the La Niña summer 1998 with negative SST anomalies in the tropical Pacific. The spatial distribution of the SST anomalies for the El Niño winter is shown Fig. 1b. Large positive SST anomalies are distributed in the tropical

TABLE 1. Description of the atmospheric GCMs utilized in the CLIVAR/Asian–Australian Monsoon GCM Intercomparison Project.

| Group | Institution | Model | Resolution | Radiation | Convection | Land surface process | Cloud formulation |
|---|---|---|---|---|---|---|---|
| COLA | Center for Ocean-Land-Atmosphere Studies (U.S.A.) | COLA 1.11 | R40L18 | Lacis and Hansen (1974) Harshvardhan et al. (1987) | Relaxed Arakawa–Schubert (RAS; Moorthi and Suarez 1992) | Simple Biosphere (SiB) model, Xue et al. (1991) | Hou (1990) based on Slingo (1987) |
| DNM | Institute of Numerical Mathematics (Russia) | A5421 | 4° × 5°, L21 | Slingo (1989) Chou et al. (1993) | Betts (1986) | Volodin and Lykossov (1998) | Slingo (1987) |
| GEOS | National Aeronautics and Space Administration Goddard Space Flight Center (U.S.A.) | GEOS-2 | 2° × 2.5°, L43 | Chou and Suarez (1994) | RAS (Moorthi and Suarez 1992) | Schemm et al. (1992) | Slingo and Ritter (1985) |
| GFDL | Geophysical Fluid Dynamics Laboratory (U.S.A.) | DERF GFDLSM V197 | T42L18 | Lacis and Hansen (1974) Schwarzkopf and Fels (1991) | RAS (Moorthi and Suarez 1992) | Deardorff (1978) | Slingo (1987), Gordon (1992) |
| IAP | Institute of Atmospheric Physics (China) | SAGCM 1.1 | R15L9 | ESFT Shi (1981) | Moist convective adjustment (MCA; Manabe et al. 1965), No shallow convection | SiB model, Xue et al. (1991) | Prescribed |
| IITM | Indian Institute of Tropical Meteorology (India) | HadAM2b V4.0, UKMO | 2.5° × 3.75°, L19 | Ingram et al. (1996) Slingo and Wilderspin (1986) | Mass flux penetrative convection scheme (Gregory and Rowntree 1990) | Smith (1993) | Smith (1990) |
| MRI | Meteorological Research Institute (Japan) | MRI GCM2 | 4° × 5°, L15 | Lacis and Hansen (1974) Shibata and Aoki (1989) | Arakawa–Schubert, Tokioka et al. (1988) | Katayama (1978), Kitoh et al. (1988) | Tokioka et al. (1984) |
| NCAR | National Center for Atmospheric Research (U.S.A.) | CCM3 | T42L18 | Kiehl et al. (1998) | Mass flux scheme (Zhang and McFarlane 1995) | Land surface model (Bonan 1998) | Slingo (1987), Kiehl (1994) |
| NCEP | National Centers for Environmental Prediction (U.S.A.) | Seasonal MRF vsn0 | T42L28 | Chou et al. (1992) Fels and Schwarzkopf (1975) | RAS (Moorthi and Suarez 1992) | Pan and Mahrt (1987) | Slingo (1987), Campana et al. (1994) |
| SNU | Seoul National University (Korea) | SNU V.2 | T31L20 | Nakajima and Tanaka (1986) | Simplified RAS, Diffusion-type shallow convection | Land surface model (Bonan 1998) | Le Treut and Li (1991) |
| SUNY | State University of New York (U.S.A.) | GLA GCM - 01.0 | 4° × 5°, L17 | Harshvardhan et al. (1987) | Modified Arakawa–Schubert | Deardorff (1978) | Sud and Walker (1992) |

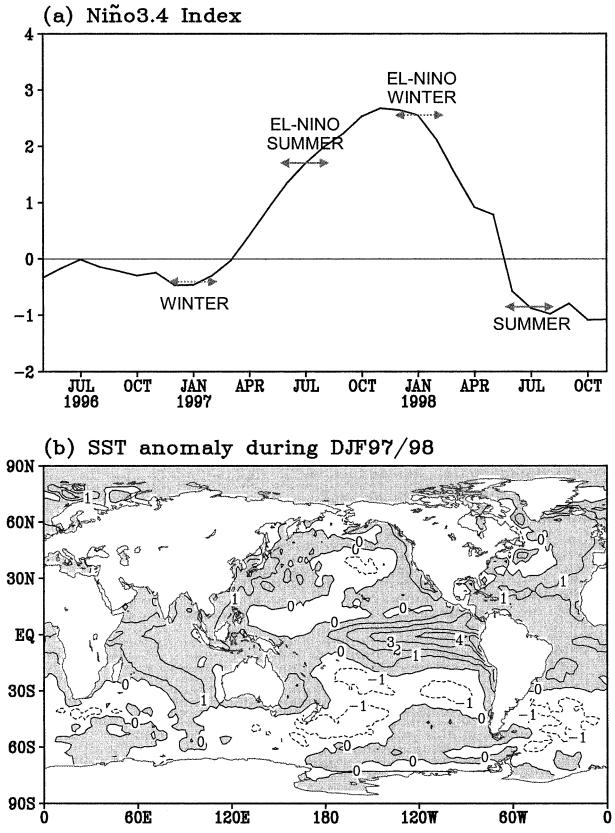


FIG. 1. (a) Time evolution of the Niño-3.4 index for Jun 1996–Oct 1998. (b) Distribution of the SST anomalies for the 1997/98 El Niño winter.

eastern and central Pacific with a maximum value of more than 4°C. Smaller positive anomalies are also seen in the other oceans: the Indian Ocean, the eastern North Pacific, and the Atlantic Ocean in the Northern Hemisphere Tropics. In addition, negative anomalies are found in the Southern Hemisphere oceans and in the central North Pacific.

The overall performance of the GCMs in simulating the atmospheric anomalies associated with the tropical SST anomalies can be examined in terms of the Southern Oscillation index (SOI), which correlates negatively with the SST variations associated with El Niño events (Trenberth 1976; Horel and Wallace 1981). The SOI of each model is calculated by subtracting the sea level pressure (SLP) anomaly averaged over 5°S–5°N and 125°–135°E from the SLP anomaly averaged over 5°S–5°N and 145°–155°W based on the ensemble mean data of 10 runs with the model. The model index is compared to the SOI obtained using the NCEP–NCAR reanalysis data (Kalnay et al. 1996). Hereafter, the statistics from the reanalysis data will be referred to as the observed, although it is understood that they are not exactly the same as the observations. Figure 2 shows the SOIs from each model and from the observed data. The observed SOI has relatively small positive values for 1996, negative values after spring 1997 as the onset timing of 1997/98 El Niño, and the large negative values after summer 1997 until spring 1998. The variation of the SOI is generally in accordance with the Niño-3.4 index shown in Fig. 1a, except for the difference in sign. A comparison of the characteristics of the observed SOI with those simulated by the models indicates that all the

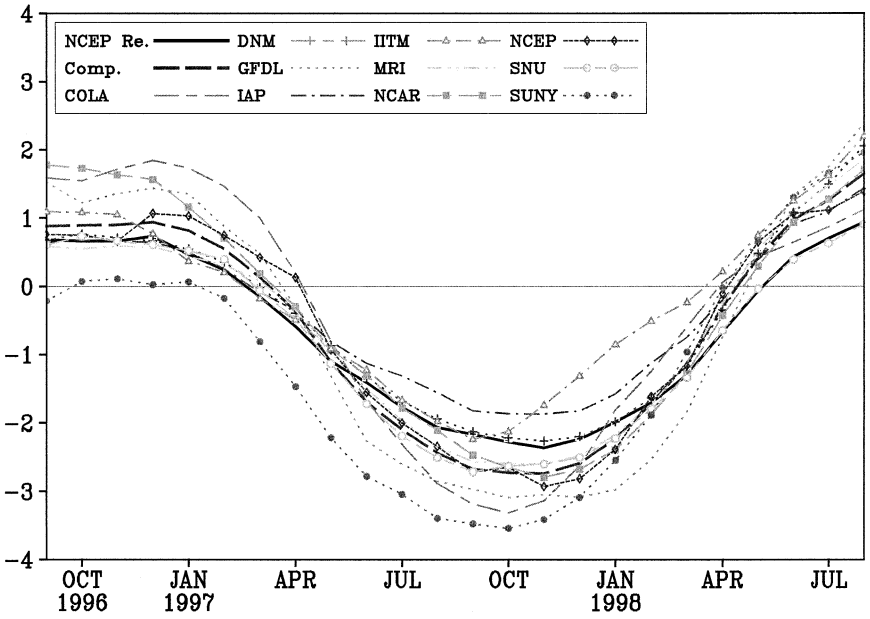


FIG. 2. Southern Oscillation index (SOI) for Sep 1996–Aug 1998. Observed SOI is shown by the thick solid line, and the model composite index is shown by the thick dashed line. The line patterns for the SOI of the individual models are indicated in the legend at upper left.

models respond sensitively to the tropical Pacific SST in a way similar to the observed, although each model produces a slightly different phase and amplitude of the index. In general, models overestimate the SOI during the El Niño except for the IAP model. Although there is some spread in the model SOI, the composite value shown in Fig. 2 varies closely with the observed SOI. This result indicates that the present GCMs as a whole are able to mimic the tropical atmospheric anomalies associated with the evolution of the recent El Niño.

## 3. Precipitation anomalies

It is expected that the rainfall distribution simulated by the models is closely related to the prescribed SST. This close relationship has been demonstrated by a number of previous studies (e.g., Horel and Wallace 1981; Ropelewski and Halpert 1987; Halpert and Ropelewski 1992). In the present section, we examine the precipitation anomalies simulated by 11 models and specifically consider the systematic error of the models, the spread relative to the observed anomalies, and how the precipitation anomalies are linked to the SST anomalies, particularly in the tropical Pacific. For this purpose, all model composites of seasonal-mean rainfall anomalies were calculated first and then compared with the corresponding observations. The observed precipitation data are the CPC Merged Analysis of Precipitation [CMAP; see documentation by Xie and Arkin (1997)] from NCEP.

The right-hand side of Fig. 3 shows the precipitation anomalies of all model composites for the two winters and two summers in the period from September 1996 to August 1998. The corresponding CMAP precipitation anomalies are shown in the left-hand side of Fig. 3. The winter mean precipitation observed for the winter of December 1996–February 1997, when the tropical Pacific was in a normal state, shows positive anomalies over the Maritime Continent and negative anomalies over the central tropical Pacific (Fig. 3a). The simulated anomalies for the corresponding period show a distribution similar to those of the observed, although the magnitudes of the simulated anomalies are much weaker, particularly over the Maritime Continent. The spatial correlation between the two maps is 0.55 for the tropical region between 30°S and 30°N. Although similar, it may not be possible to say what is ''forced'' by the SST anomalies and what is simply due to the averaging of a small number of chance fluctuations. This issue is addressed by performing a simple Student's *t* test, and then the regions of statistical significance at the 99% level are highlighted by shading in the figures. The results of the Student's *t* test indicate that the large-scale precipitation anomalies simulated in the Tropics are closely related to the SST anomalies not only for the El Niño period (Figs. 3d,f) but also for the seasons of weak SST anomalies (Figs. 3d,h).

For the El Niño period covering the 1997 summer and 1997/98 winter, the simulated and observed anomalies are very similar (Figs. 3c–f). In particular, the model composites reproduce many features of the observed precipitation anomalies in the equatorial central and eastern Pacific. However, some discrepancies appear in the Maritime Continent, where the observed negative anomalies are poorly simulated, particularly for the El Niño winter. (As will be seen later in Fig. 6, most of the models have difficulties in simulating the negative anomalies in the Maritime Continent properly.) Even though the tropical Pacific SST anomalies were relatively weak during the summer of 1998, the spatial pattern of the observed anomaly is reasonably well reproduced by the model composite (Fig. 3h). The results in Fig. 3 indicate that the precipitation anomalies, specifically in the tropical oceans are closely related to the SST anomalies, and this relationship is reproduced reasonably well by the model composite. However, the models underestimate the precipitation anomalies in the Maritime Continent, particularly during the El Niño period.

Next, we examine the performance of each model in simulating the precipitation anomalies in the monsoon–ENSO region, defined by the area of 60°E–90°W and 30°S–30°N. This region covers the Asian–Australian monsoon region and the entire tropical Pacific, where large precipitation anomalies appear during El Niño events. Figure 4a shows the pattern correlation over the monsoon–ENSO region between the simulated and observed precipitation anomalies of each season. As expected, the pattern correlation has a relatively large value during the El Niño seasons. All of the models, except MRI, have the largest correlation value during the 1997/98 winter season. During this period, the correlation value for the ensemble mean of each model is in the range between 0.56 and 0.81. Not only the ensemble mean but also each individual run has a significantly large value of the correlation coefficient during the El Niño seasons. The range of correlation values of the individual runs is considerably narrower for the El Niño seasons than for the normal seasons of 1996/97 winter and 1998 summer. The pattern correlations of the composites during the El Niño seasons exceed 0.7.

Even for the seasons of weak SST anomalies December–January–February 1996–97 (DJF96/97) and June–July–August 1998 (JJA 98), the precipitation anomalies simulated by all the individual runs are positively correlated with the observed counterpart with the exception of the 1997 summer simulation by the IAP model. For these seasons, the pattern correlation of the ensemble mean exceeds 0.3 for most of the models, and the correlation value of the composite map of 11 models is near 0.5. These results indicate that a large part of observed precipitation anomalies are related to the SST anomalies regardless of their magnitude. The figures also show that, regardless of the season, the correlation value of the ensemble mean of each model is larger than that of any individual run with few exceptions, and the

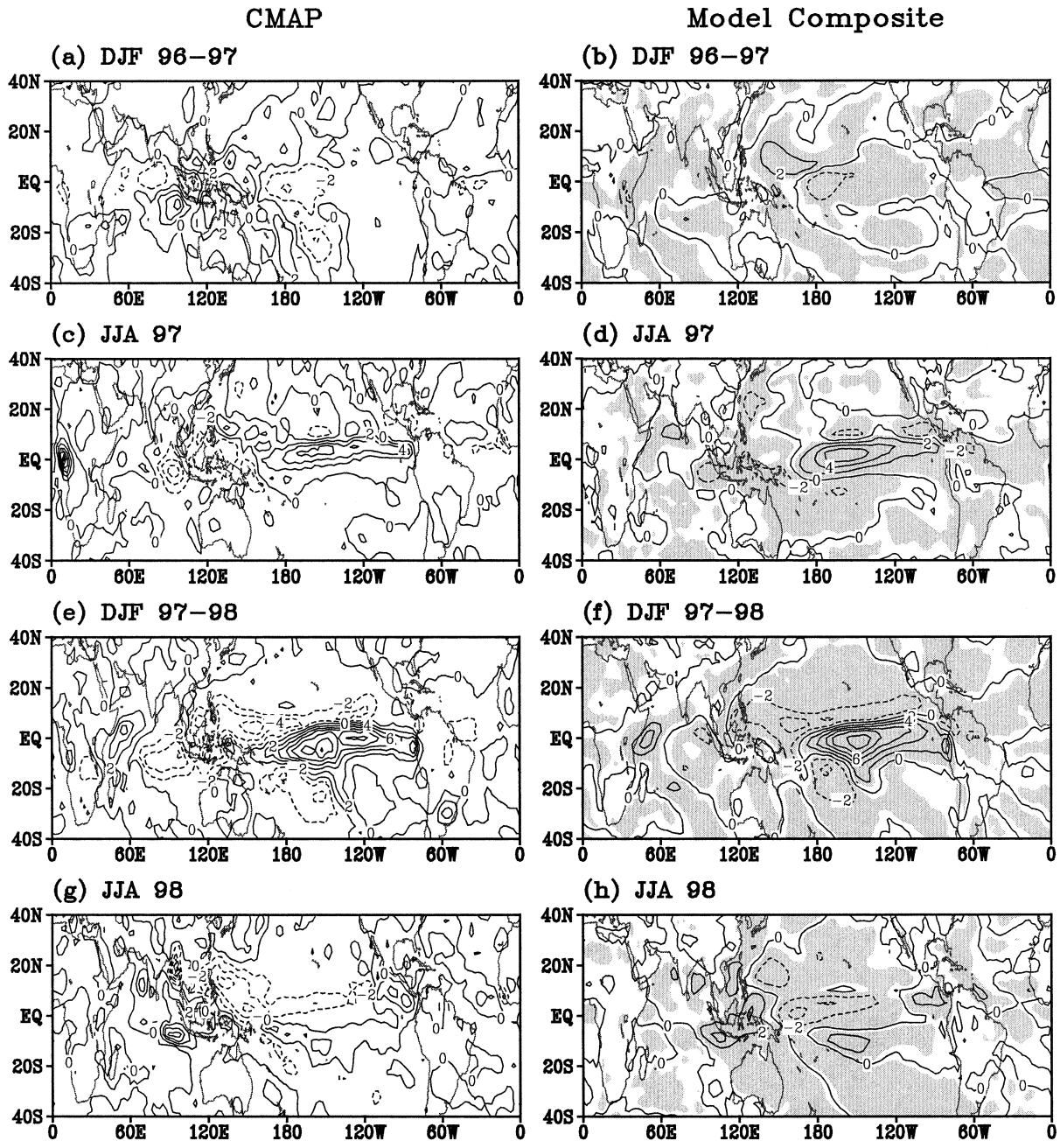


FIG. 3. Precipitation anomalies for the two winter and two summer seasons in the period between Sep 1996 and Aug 1998. (left) Observed CMAP anomalies and (right) model composites. Shading indicates the anomalies that are significant at the 99% level.

correlation value of the model composite is larger than that of the ensemble mean of individual models, with the exception of the GFDL 1997/98 winter simulation. Therefore, it is put forward that the ensemble mean and composite anomaly are usually superior to that of any individual model run (Hulme et al. 1993; Gates et al. 1999; Krishnamurti et al. 2000).

The intensity of the simulated anomaly compared to observations is examined in Fig. 4b, which shows the root-mean-square (rms) of precipitation anomalies over the monsoon–ENSO region normalized by the observed rms. If the normalized rms shown in Fig. 4b is smaller (larger) than 1, it denotes that the mean intensity of simulated anomaly is smaller (larger) than that of the observation. The precipitation anomalies simulated by the models of COLA, GFDL, IITM, and SUNY are generally larger than the observed, whereas the models of DNM, IAP, and MRI tend to simulate the anomalies weaker than the observed. The composite anomalies of 11 models are shown to be weaker than the observations

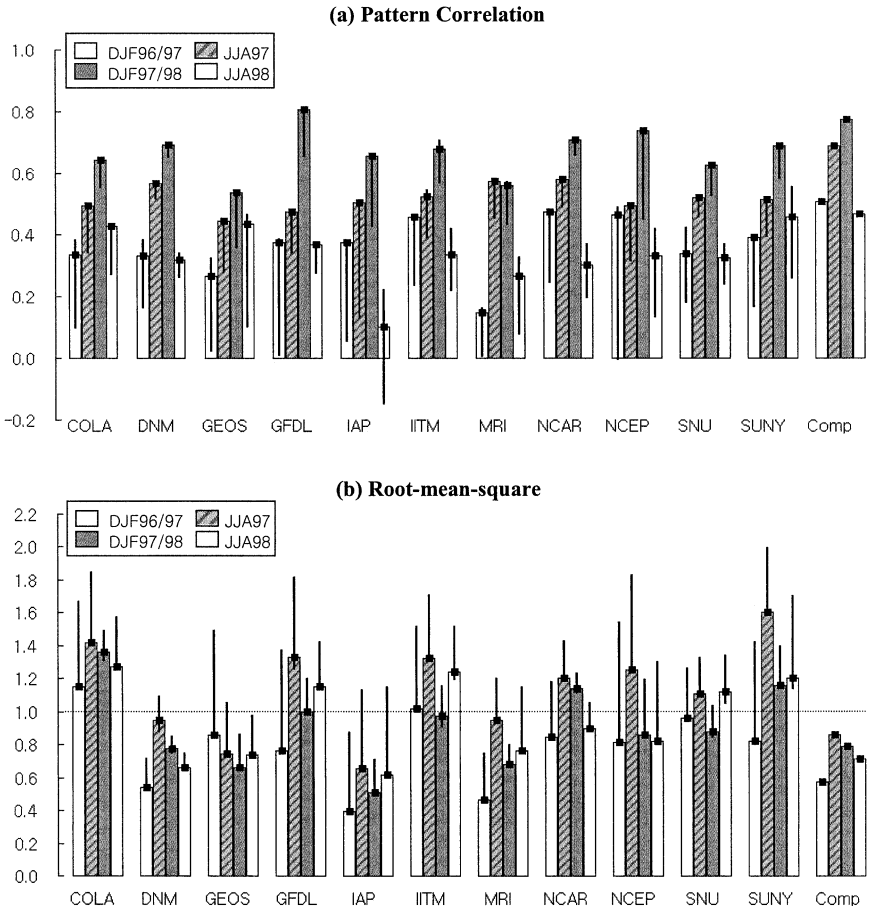


FIG. 4. (a) Pattern correlation coefficient between the simulated and observed precipitation anomalies for each model and each season over the monsoon–ENSO region, 30°S–30°N and 60°E–90°W. The line in the bar indicates the range of correlation values of each individual run, and the black square indicates the correlation of the ensemble mean. (b) Root-mean-square (rms) of the simulated precipitation anomalies over the monsoon–ENSO region, normalized by the observed rms. The line in the bar indicates the range of rms values of each individual run, and the black square indicates the rms value of the ensemble mean.

for all seasons. The normalized rms of the anomalies for the 1997 El Niño summer is generally larger than the 1997/98 El Niño winter for all of the models without exception. The simulated anomaly being larger during the summer is also true for the normal years.

It is also interesting to examine how the anomalies of each model during the El Niño seasons are related to the accuracy of the model climatology. To address this issue, the pattern correlation between the observed climatology and the climatology of each model for the monsoon–ENSO region were calculated and plotted against the pattern correlation of the anomalies. Figure 5a shows a scatter diagram of the pattern correlation of climatology ($x$ axis) versus the pattern correlation of anomaly ($y$ axis). As seen in Fig. 4, the 1997/98 winter anomaly simulations are generally better than those of 1997 summer. Figure 5a illustrates that there is no clear relationship between the degree of accuracy of the climatology and that of the anomaly for both seasons, although the best model of the anomaly coincides with the best model of the climatology for each season. On the other hand, Fig. 5b shows that for both seasons, the intensity of simulated anomaly is generally proportional to the intensity of the corresponding climatology of each model. In other words, the models with a larger (smaller) climatological mean precipitation than the observed generally simulate larger (smaller) El Niño anomalies than the observed. It implies that a simple bias correction of anomalies can be made based on the quality of the model climatology.

To focus on the simulation of the 1997/98 El Niño winter, the ensemble mean precipitation anomaly of each model is shown in Fig. 6. The Student's $t$ test is also performed for each model and the anomalies of significance level at 99% are shaded in the figures. Figures show that most models reproduce the precipitation anomalies in the tropical Pacific, which are significantly related to the prescribed SST anomalies. Whereas, the

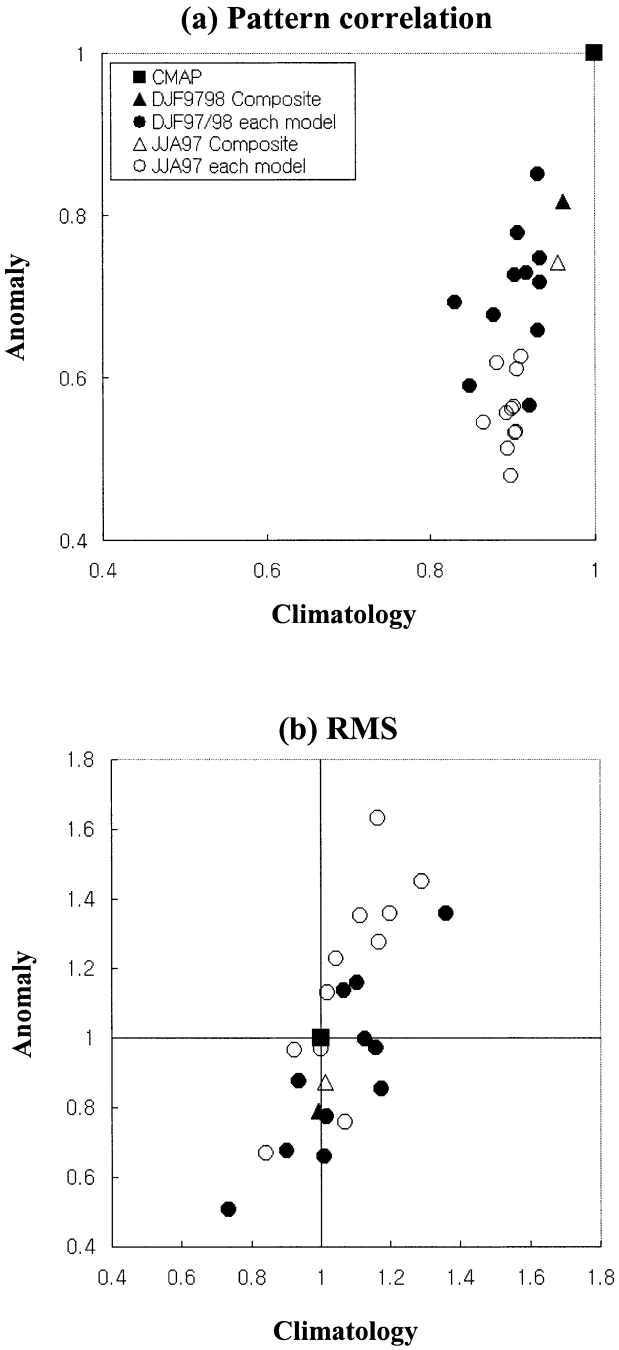


FIG. 5. (a) Scatterplot of the pattern correlation of the ensemble anomalies of each model over the monsoon–ENSO region vs that of the corresponding climatology for the 1997 summer and 1997/98 winter seasons. (b) As in (a) except for the normalized rms. Open and dark symbols are for the 1997 summer and 1997/98 winter, respectively.

simulated precipitation anomalies in Indian and East Asian regions are poorly related to the SST anomalies.

For comparison, the observed CMAP precipitation anomaly is also shown in Fig. 6a. The models, as a whole, produce a broadly realistic distribution of precipitation anomalies. But the intensity of the anomalies in the equatorial Pacific and Maritime Continent shows large intermodel differences. The ENSO-related positive anomalies in the equatorial central Pacific (Horel and Wallace 1981) simulated by GEOS and IAP are very weak compared to the observed counterpart. On the other hand, COLA, NCAR, and SUNY models produce larger positive anomalies in the same region. All the models, except GFDL, poorly simulate the observed negative anomalies over the western Pacific near Indonesia, which is also the region of greatest disagreement among the models. Except over this region, the composite of the 11 model anomalies, shown in Fig. 3f, is in good agreement with the observed counterpart over the Tropics and even in the northern extratropics, particularly over North America.

We also examined how the composite field varies with different combinations of the model anomalies during the 1997/98 El Niño season. This examination is motivated to sort out the optimal combination of models. Figure 7 shows the range of the correlation coefficient between the model composite and the observed precipitation anomalies in the monsoon–ENSO region for different numbers of composite members. For a single model, the values range from 0.56 to 0.85. For two-model composites, the values range from 0.66 to 0.86, and for all 11 models the correlation reaches 0.83. The figure shows that the maximum correlation value changes little, while the minimum value increases significantly with an increase of the number of models. A close examination evinces that the maximum value actually decreases slightly with more than three models, indicating that the best model or a composite of a few models can be better than the composite of many models. It may be interesting to find out which combination of models produces a relatively high-correlation value, particularly for the composite of three models. As shown in Table 2, the best combination is obtained by the composite of GFDL, IAP, and NCEP models. The GFDL model always gets included in combinations of the top 10 correlation values because of its ability to produce the highest pattern correlation of the precipitation anomalies, as seen in Fig. 4a. The IAP model, which simulated the ENSO anomalies poorly (Fig. 6), is included in many cases of top 10 combinations. These results indicate that a better composite is not made by a combination of best models but can be obtained by a combination of various kinds of models including the models of relatively poor performance, but independent from other models. It is pointed out, however, that a superensemble method recently developed by Krishnamurti et al. (2000) may produce a different result from that shown in Fig. 7, since the method assigns weights to the models according to their skill.

## 4. 200-hPa geopotential height anomalies

This section examines the upper-tropospheric circulation anomalies associated with the precipitation anom-

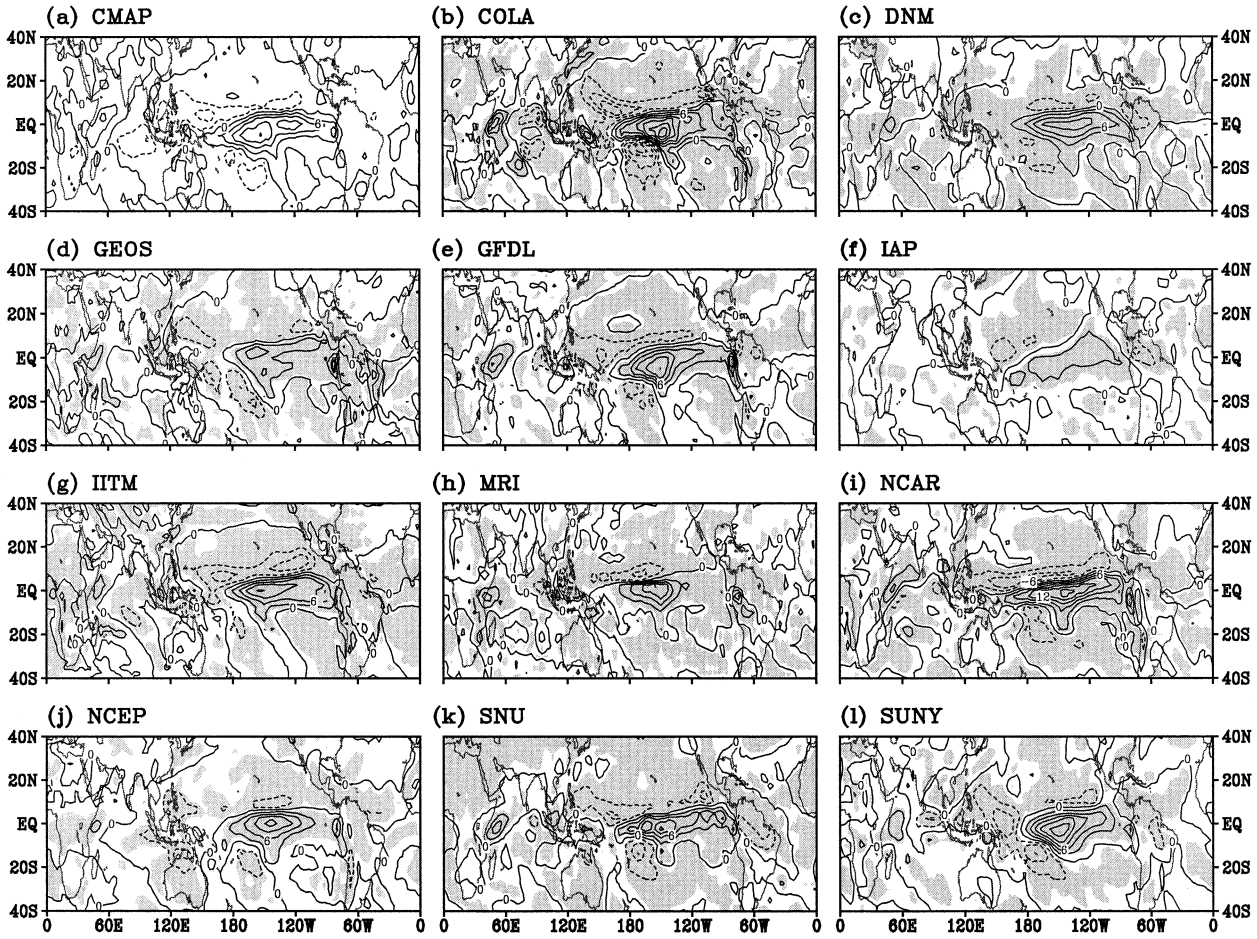


FIG. 6. Distribution of precipitation anomalies during the 1997/98 winter for the (a) CMAP, and (b)–(l) for the ensemble mean of each model. Shaded area denotes anomalies that are significant at the 99% level.

alies discussed earlier, with emphasis on the El Niño seasons. Since GEOS and IITM have not provided the geopotential height data, the data from COLA, DNM, GFDL, IAP, MRI, NCAR, NCEP, SNU, and SUNY models are used for the analysis of the geopotential height. The NCEP–NCAR reanalysis data (Kalnay et al. 1996) are used for the observed counterpart. Figure 8a shows the 200-hPa geopotential height anomalies during the 1997 summer, obtained as an average of the nine-model ensemble means. A distinctive anomaly pattern appears in the Southern Hemisphere (SH) Pacific with a wave train emanating from the tropical central Pacific. The anomalies of statistical significance at the 99% level are confined in the regions of the wave train. The model anomalies in the Northern Hemisphere (NH) appear to be very weak. However, relatively large anomalies appear all over the NH in the observations (Fig. 8b). Although the individual model runs also show substantial anomalies in NH, they are cancelled out in the composite, indicating that the observed anomalies in the NH are related to transients. Discrepancies between the model and observations also appear in the SH, particularly in the polar region. Note that the wave train in the Pacific also appears in the observations.

The geopotential anomalies during the 1997/98 winter are also shown in Figs. 8c and 8d for the model composite and the NCEP–NCAR reanalysis, respectively. The spatial pattern of the observed anomalies in the Tropics and the PNA region are reasonably well reproduced by the model composite, although the model anomalies are weaker than the observed, particularly in the PNA region. Large discrepancies between the model and observed anomalies are also apparent in the high latitudes of the Asian continent. The statistically significant anomalies of the model composite are found all over the Tropics and in the PNA region, where the model composite is qualitatively similar to the observed counterpart.

The performance of each model in simulating the NH circulation anomalies for the El Niño winter is now examined. Figure 9 shows the ensemble means of 200-hPa geopotential height anomalies simulated by each model. The anomaly distributions of NCEP–NCAR reanalysis and the model composite are also included in

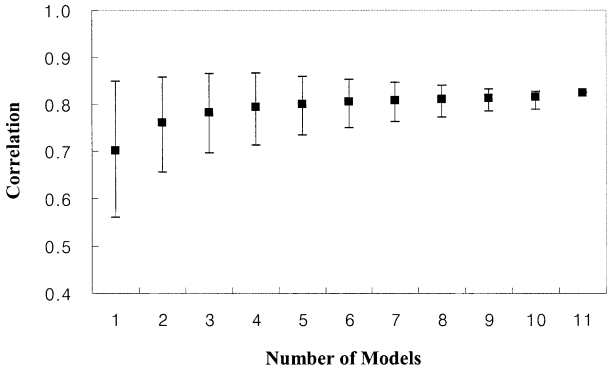


FIG. 7. Range of pattern correlation values between the observed and model composite precipitation anomalies over the monsoon–ENSO region for different numbers of the models being composed during the 1997/98 winter. The black square indicates the average value of the correlation coefficients for various combinations of the models composed.

TABLE 2. Model combinations for the highest 10 correlations for three-model composites.

| Composite members | | | Correlation |
|---|---|---|---|
| GFDL | IAP | NCEP | 0.866 |
| GFDL | IAP | DNM | 0.862 |
| GFDL | DNM | NCEP | 0.859 |
| GFDL | IAP | IITM | 0.856 |
| GFDL | IITM | NCEP | 0.856 |
| GFDL | NCAR | NCEP | 0.851 |
| GFDL | IAP | NCAR | 0.850 |
| GFDL | SUNY | NCEP | 0.843 |
| GFDL | IITM | DNM | 0.841 |
| GFDL | IAP | SNU | 0.839 |

Fig. 9. The models, as a whole, are seen to produce a broadly realistic distribution of anomalies, but there are large disagreements among the models in the amplitudes. In particular, the models such as IAP and MRI simulate circulation anomalies that are much weaker than those in observations and the other models. The Student's *t* test of each model composite indicates that the simulated tropical anomalies are significantly related to the SST anomalies for all models. Whereas the extratropical anomalies of significance are more or less confined in the PNA region, particularly the negative anomalies off the east coast of Alaska and the positive anomalies over eastern Canada, although the locations of significant anomalies are slightly different from one model to another.

Most of the models generally underestimate the observed anomalies, especially in the PNA region. This underestimation is clearly illustrated by Fig. 10 in which the geopotential anomalies normalized by the observed rms over the PNA region, are plotted against the pattern correlations between the model and observed anomalies in the PNA region. Hereafter, the PNA region is defined as the region of 180°E–60°W and 20°–80°N. The normalized rms is less than 1 for all of the models, indicating the underestimation. This underestimation may result from the internal (unforced) variability inherent in the observations, which are largely cancelled out by the ensemble in the model results. The pattern correlation is generally large for most of the models except

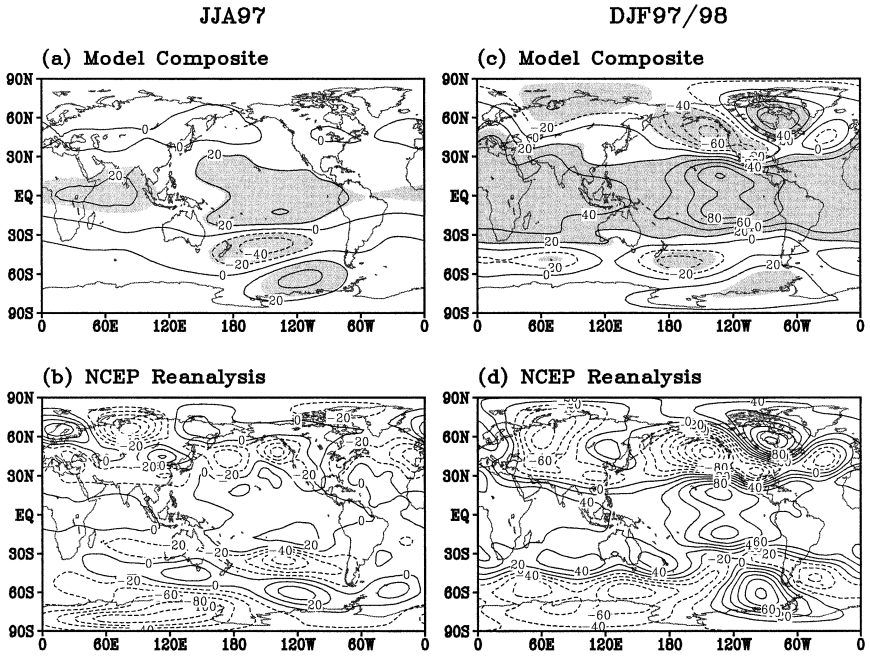


FIG. 8. Global distribution of 200-hPa geopotential height anomalies: (a), (b) model composites and the NCEP–NCAR reanalysis during the 1997 summer, respectively; and (c), (d) the 1997/98 winter. Shading indicates the anomalies that are significant at the 99% level.

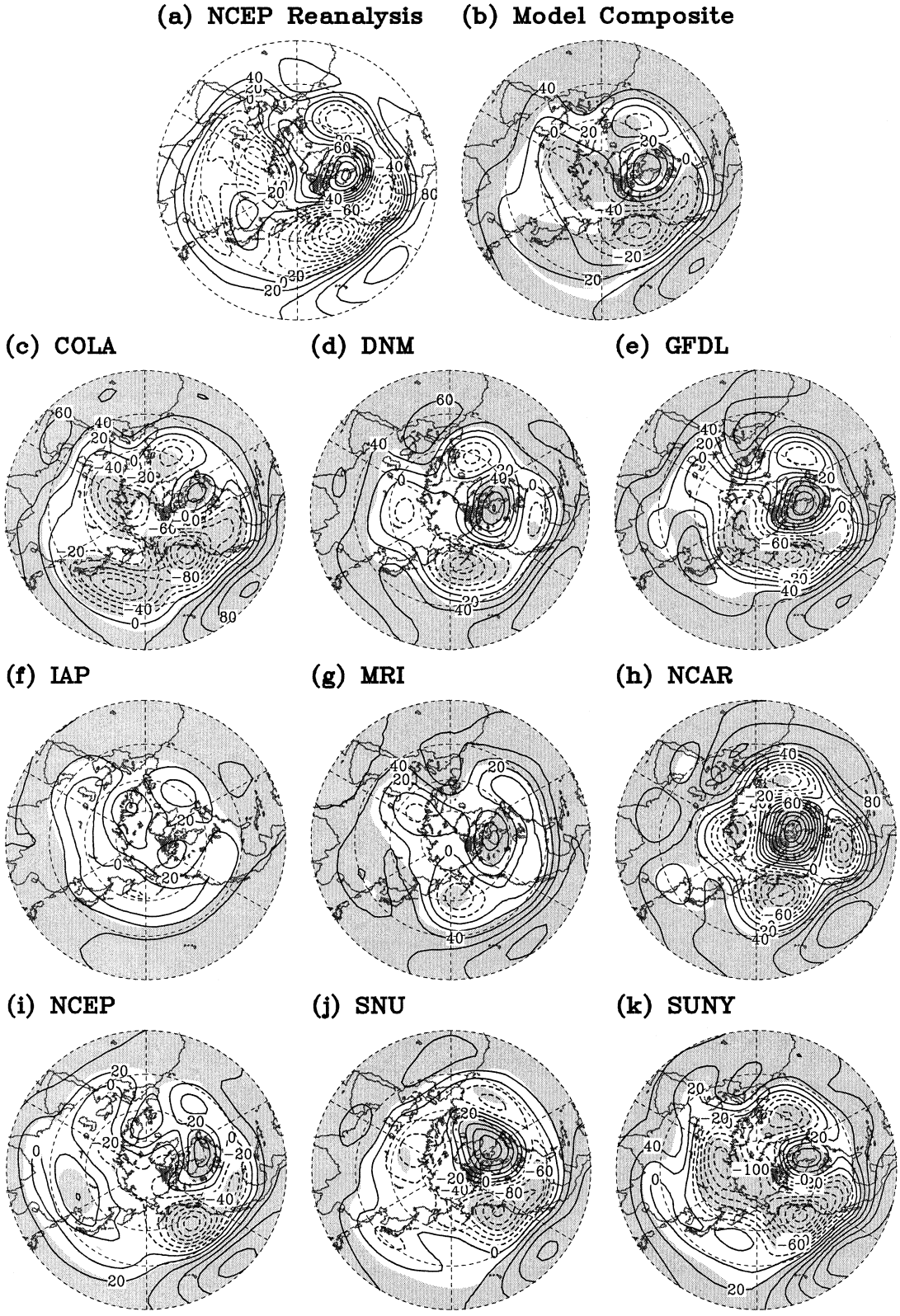


FIG. 9. Distribution of 200-hPa geopotential height anomaly over the Northern Hemisphere north of 10°N during the 1997/98 winter: (a), (b) the NCEP–NCAR reanalysis and the model composite, respectively. (c)–(k) The ensemble mean of each model; shaded area denotes anomalies that are significant at the 99% level.

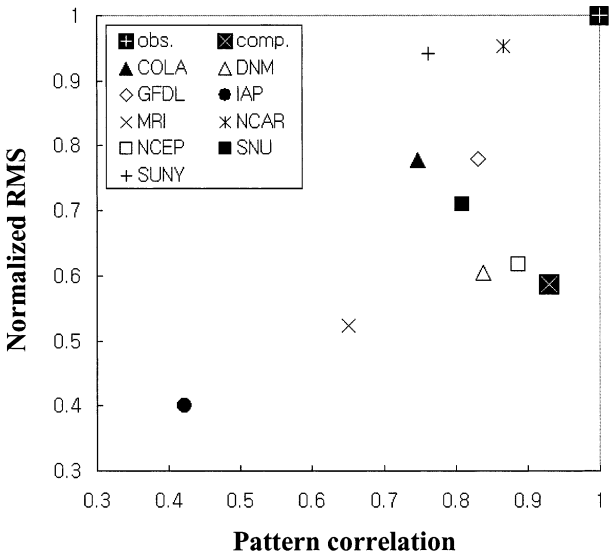


FIG. 10. Scatterplot of the pattern correlation between the model and observed anomalies (*x* axis) vs the normalized rms (*y* axis) of 200-hPa geopotential height anomalies over the PNA region during the 1997/98 winter season. The values for the ensemble mean of each model and the model composite are indicated by the symbols shown in the legend at upper left.

the IAP and MRI models. It is interesting to note that the models with a lower correlation value simulate weaker anomalies. Overall, the present results indicate that the present GCMs simulate the PNA pattern with a reasonably good structure but with weaker intensity.

The relationship between the tropical precipitation and the PNA pattern simulated by the models is now examined using Fig. 11. In Fig. 11a, the pattern correlation of 200-hPa geopotential height anomalies of each model with those of NCEP–NCAR reanalysis over the PNA region are plotted against the pattern correlation between the model and observed precipitation anomalies over the monsoon–ENSO region during the El Niño winter. It shows that the two correlation values are linearly proportional to each other, indicating that the circulation anomalies in the PNA region are directly related to the tropical precipitation anomalies during ENSO. The relationship between the amplitudes of tropical precipitation and the PNA pattern also shows that the amplitude of the PNA pattern is proportional to that of the tropical precipitation anomaly (Fig. 11b). Both figures indicate that a better simulation of the PNA pattern depends on a better representation of precipitation anomalies in the tropical Pacific.

Also examined is the relationship between the simulated circulation anomalies in the NH and SH extratropics during the El Niño winter. Figure 12a shows the pattern correlations between the observed and simulated geopotential anomalies in the PNA region versus those in the SH extratropics in the region of 180°E–60°W and 20°–80°S. Again, the NCEP–NCAR reanalysis is used as an observation although the reanalysis data may not

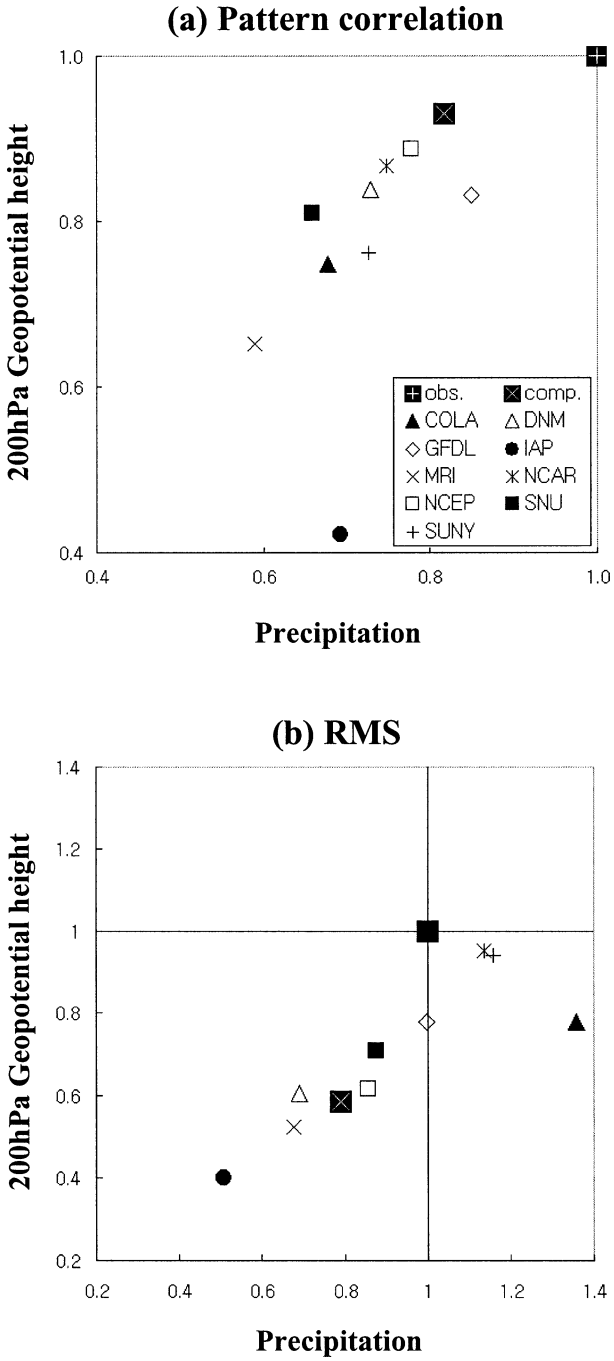


FIG. 11. (a) Scatterplot of the pattern correlation between the model and the NCEP–NCAR reanalysis anomalies for the 200-hPa geopotential height over the PNA region (*y* axis) vs similar pattern correlation of precipitation anomalies over the monsoon–ENSO region during the 1997/98 winter season (*x* axis). (b) As in (a) except for the normalized rms.

represent the actual observation, particularly in the Southern Hemisphere. Interestingly, there is no clear relationship between the pattern correlations of the NH and SH circulation anomalies associated with the ENSO, indicating that the model that better simulates the NH

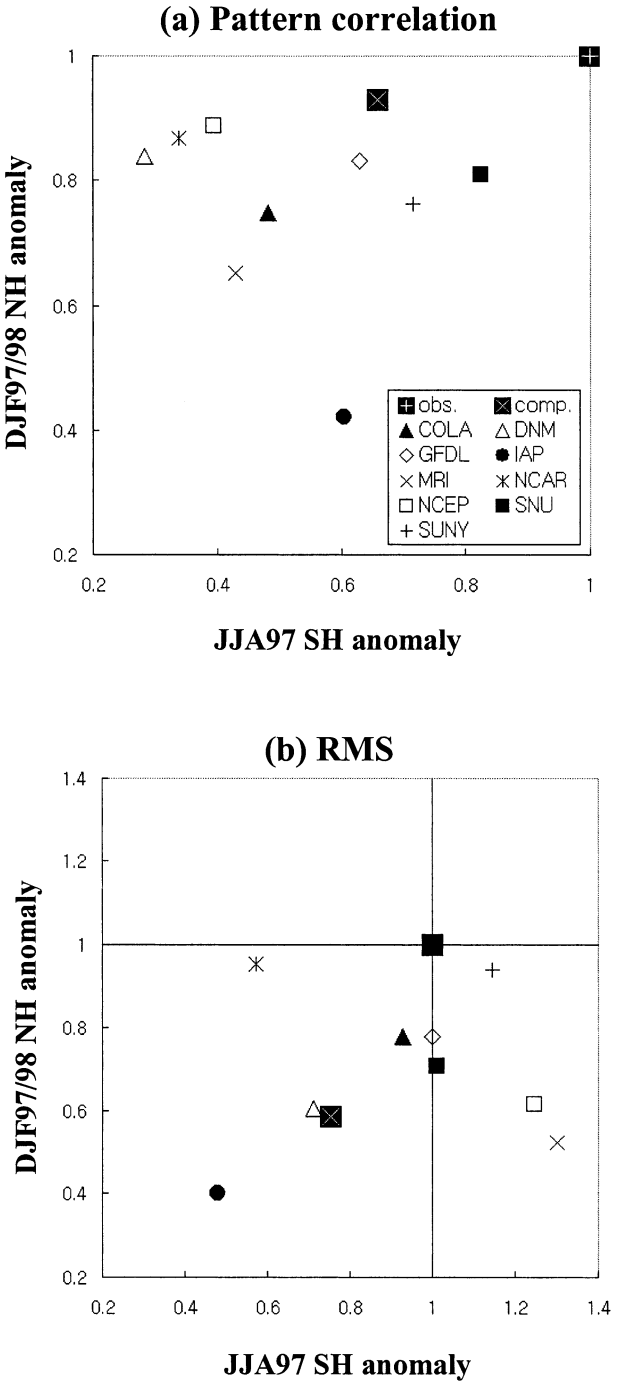


FIG. 12. As in Fig. 11 except for the Northern Hemisphere anomalies during the 1997/98 winter (*y* axis) and the Southern Hemisphere anomalies during the 1997 summer (*x* axis).

anomalies does not necessarily produce a better simulation of the SH anomalies. Most of the models also show poor ability in the simulation of the SH anomalies compared to that of the NH anomalies. The SNU model appears to simulate both NH and SH anomalies reasonably well. In contrast to the pattern correlation, there appears a linear relationship between the amplitudes of anomalies in the PNA region and those in the SH region (Fig. 11b), in spite of some exceptions such as the models of NCAR, NCEP, and MRI. Figure 12 indicates that, during the El Niño winter, the amplitudes of the extratropical circulation anomalies in the SH and NH are generally controlled by the same tropical precipitation anomalies. Such a variable pattern in the SH may be due to a large impact of transients in the SH, and part of the NH anomalies may be due to the influence of stationary waves in the circulation anomalies (Simmons et al. 1983; Branstator 1985).

## 5. Summary and discussion

This paper has presented an overview of the results of the Asian–Australian Monsoon GCM Intercomparison Project with a focus on the global ENSO anomalies during 1997/98 period, particularly the tropical rainfall anomalies and the upper-tropospheric circulation anomalies in the Pacific–North American region. The GCM data analyzed are a set of 10 ensemble simulations for 1 September 1996–31 August 1998 from the participating modeling groups of 11 institutions. In particular, this paper examines the performance of the state-of-art models as a whole and seeks to summarize the characteristics of the model simulations for the recent El Niño period. Thus, the analysis presented here was not intended to establish the ultimate superiority of one model over another.

Although there are apparent model outliers in each simulated variable examined, validation of the model composite shows that the average large-scale seasonal distributions of precipitation and geopotential height are reasonably close to what are believed to be the best observational estimates available. But, it also shows large intermodel differences in the centers of response to the tropical SST anomalies associated with the 1997/98 El Niño. In the case of precipitation anomaly, large intermodel differences appear over the tropical central Pacific and the Maritime Continent. All the models simulate the spatial pattern of the observed El Niño anomalies in the tropical central Pacific reasonably well during El Niño, although their amplitudes show large intermodel differences. On the other hand, most of the models have difficulty in simulating the negative anomalies over the Maritime Continent during the El Niño. It is noted that any physical insight of the common GCM problems has not been provided in the present study. Therefore, continued investigations into the model differences and common problems are needed to improve the current GCMs.

The upper-tropospheric circulation anomalies observed during the 1997/98 winter show a distinct wave train in the PNA region, emanating from the tropical Pacific. Such a phenomenon also appeared in the Southern Hemisphere for the 1997 summer. Most of the models reproduce the observed spatial pattern of the 200-hPa geopotential anomalies over the PNA region. How-

ever, the models generally underestimate the amplitude of the ENSO anomalies in the PNA region. In particular, the PNA pattern simulated by the models such as IAP and MRI are significantly weaker than the observed, and those weak amplitudes are related to the weak precipitation anomalies in the tropical Pacific. Most of the models have a linear relationship between the tropical precipitation anomalies and the circulation anomalies in the PNA region. It was also noted that a model that simulates the NH anomalies better does not necessarily produce a better simulation of the SH anomalies. The simulations of SH anomalies show large disagreements among the models, suggesting that much of the SH variability is due to a large impact of transients, and that the more deterministic part of NH anomalies, particularly the PNA pattern, is due to the influence of stationary waves in the circulation anomalies (Simmons et al. 1983; Branstator 1985).

It was also noted that the tropical precipitation anomalies are closely related to the SST anomalies not only for the El Niño seasons but also for the normal seasons with weak SST anomalies in the tropical Pacific. In particular, the model composites of the simulated anomalies for the normal winter (December 1996–February 1997) and summer (June–August 1998) seasons show a reasonable degree of similarity to the observed counterparts, although the magnitudes of the simulated anomalies are weaker, particularly over the Maritime Continent. The pattern correlation values for the normal seasons between the observed and corresponding model composite are near 0.5 for the tropical region between 30°S and 30°N. This result may provide some hope to consider short-range climate forecasting as a slowly varying boundary value problem.

*Acknowledgments.* The present work is a part of the CLIVAR/Asian–Australian Monsoon Panel modeling component. The first author is supported by the Climate Environment System Research Center at Seoul National University supported by the Korea Science and Engineering Foundation and Brain Korea 21. V. Krishnamurthy and J. Shukla were supported by grants from the National Oceanic and Atmospheric Administration (NA96-GP0056) and the National Science Foundation (ATM-9814295).

## REFERENCES

Bell, G. D., M. S. Halpert, V. E. Kousky, M. E. Gelman, C. F. Ropelewski, A. V. Douglas, and R. C. Schnell, 1999: Climate assessment for 1998. *Bull. Amer. Meteor. Soc.,* **80,** 1040–1040.

Betts, A. K., 1986: A new convective adjustment scheme. Part I: Observational and theoretical basis. *Quart. J. Roy. Meteor. Soc.,* **112,** 677–691.

Blackmon, M. L., J. E. Geisler, and E. J. Pitcher, 1983: A general circulation model study of January climate anomaly associated with interannual variations of equatorial Pacific sea surface temperatures. *J. Atmos. Sci.,* **40,** 1410–1425.

Bonan, G. B., 1998: The land surface climatology of the NCAR land surface model coupled to the NCAR Community Climate Model. *J. Climate,* **11,** 1307–1326.

Boyle, J. S., 1998: Intercomparison of interannual variability of the global 200-hPa circulation for AMIP simulations. *J. Climate,* **11,** 2505–2529.

Branstator, G., 1985: Analysis of general circulation model sea-surface temperature anomaly simulations using a linear model. Part II: Eigenanalysis. *J. Atmos Sci.,* **42,** 2242–2254.

Campana, K. A., Y.-T. Hou, K. E. Mitchell, S.-K. Yang, and R. Cullather, 1994: Improved diagnostic cloud parameterization in NMC's global model. Preprints, *10th Conf. on Numerical Weather Prediction,* Portland, OR, Amer. Meteor. Soc., 324–325.

Chou, M.-D., and M. J. Suarez, 1994: An efficient thermal infrared radiation parameterization for use in general circulation models. NASA Tech. Memo. 104606, Vol. 3, Goddard Space Flight Center, Greenbelt, MD, 84 pp.

——, G. Ji, K.-N. Liou, and S.-C. S. Ou, 1992: Calculations of surface radiation in Arid regions—A case study. *J. Appl. Meteor,* **31,** 1084–1095.

——, W. Ridgway, and M.-H. Yan, 1993: One-parameter scaling and exponential-sum fitting for water vapor and $CO_2$ infrared transmission functions. *J. Atmos. Sci.,* **50,** 2294–2303.

Deardorff, J. W., 1978: Efficient prediction of ground surface temperature and moisture, with inclusion of a layer of vegetation. *J. Geophys. Res.,* **83,** 1889–1903.

Fels, S. B., and M. D. Schwarzkopf, 1975: The simplified exchange approximation: A new method for radiative transfer calculations. *J. Atmos. Sci.,* **32,** 1475–1488.

Gates, W. L., and Coauthors, 1999: An overview of the results of the atmospheric model intercomparison project (AMIP1). *Bull. Amer. Meteor. Soc.,* **80,** 29–55.

Gordon, C. T., 1992: Comparison of 30-day integrations with and without cloud-radiation interaction. *Mon. Wea. Rev.,* **120,** 1244–1277.

Graham, N. E., T. P. Barnett, R. Wilde, M. Ponater, and S. Schubert, 1994: On the roles of tropical and midlatitude SSTs in forcing interannual to interdecadal variability in the winter Northern Hemisphere circulation. *J. Climate,* **7,** 1416–1441.

Gregory, D., and P. R. Rowntree, 1990: A mass flux convection scheme with representation of cloud ensemble characteristics and stability dependent closure. *Mon. Wea. Rev.,* **118,** 1483–1506.

Halpert, M. S., and C. F. Ropelewski, 1992: Surface temperature patterns associated with the Southern Oscillation. *J. Climate,* **5,** 577–593.

Harshvardhan, D. A. Randall, and T. G. Corsetti, 1987: A fast radiation parameterization for general circulation models. *J. Geophys. Res.,* **92,** 1009–1016.

Horel, J. D., and J. M. Wallace, 1981: Planetary-scale atmospheric phenomena associated with the Southern Oscillation. *Mon. Wea. Rev.,* **109,** 813–829.

Hou, Y.-T., 1990: Cloud-radiation-dynamics interaction. Ph.D. thesis, University of Maryland at College Park, 209 pp.

Hulme, M., K. R. Briffa, and P. D. Jones, 1993: General circulation model validation and climate change detection. Climatic Research Unit Rep., Norwich, United Kingdom, 24 pp. [Available from Climatic Research Unit, School of Environmental Sciences, University of East Anglia, Norwich NR4 7TJ, United Kingdom.]

Ingram, W. J., S. Wood Ward, and J. Edward, 1996: Radiation. Unified Model Documentation Paper 23, 83 pp.

Kalnay, E., and Coauthors, 1996: The NCEP/NCAR 40-Year Reanalysis Project. *Bull. Amer. Meteor. Soc.,* **77,** 437–471.

Katayama, A., 1978: Parameterization of the planetary boundary layer in atmospheric general circulation models (in Japanese). Kisyo Kenkyu Note 134, Meteorological Society of Japan, 153–200.

Kiehl, J. T., 1994: On the observed near cancellation between longwave and shortwave cloud forcing in tropical regions. *J. Climate,* **7,** 559–565.

——, J. J. Hack, G. Bonan, B. Boville, D. Williamson, and P. Rasch, 1998: The National Center for Atmospheric Research Community Climate Model (CCM3). *J. Climate,* **11,** 1131–1149.

Kitoh, A., K. Yamazaki, and T. Tokioka, 1988: Influence of soil moisture and surface albedo changes over the African tropical rain forest on summer climate investigated with the MRI GCM-I. *J. Meteor. Soc. Japan,* **66,** 65–86.

Krishnamurti, T. N., C. M. Kishtawal, Z. Zhang, T. LaRow, D. Bachiochi, E. Williford, S. Gadgil, and S. Surendran, 2000: Multimodel ensemble forecasts for weather and seasonal climate. *J. Climate,* **13,** 4196–4216.

Lacis, A. A., and J. E. Hansen, 1974: A parameterization for the absorption of solar radiation in the Earth's atmosphere. *J. Atmos. Sci.,* **31,** 118–133.

Lau, N.-C., 1985: Modeling the seasonal dependence of the atmospheric response to observed El Niños in 1962–76. *Mon. Wea. Rev.,* **113,** 1970–1996.

——, and M. J. Nath, 1994: A modeling study of the relative roles of tropical and extratropical SST anomalies in the variability of the global atmosphere–ocean system. *J. Climate,* **7,** 1184–1207.

Le Treut, H., and Z.-X. Li, 1991: Sensitivity of an atmospheric general circulation model to prescribed SST changes: Feedback effects associated with the simulation of cloud optical properties. *Climate Dyn.,* **5,** 175–187.

Manabe, S., J. Smagorinsky, and R. F. Strickler, 1965: Simulated climatology of a general circulation model with a hydrologic cycle. *Mon. Wea. Rev.,* **93,** 769–798.

Moorthi, S., and M. J. Suarez, 1992: Relaxed Arakawa–Schubert: A parameterization of moist convection for general circulation models. *Mon. Wea. Rev.,* **120,** 978–1002.

Nakajima, T., and M. Tanaka, 1986: Matrix formulation for the transfer of solar radiation in a plane-parallel scattering atmosphere. *J. Quant. Spectrosc. Radiat. Transfer,* **35,** 13–21.

Palmer, T. N., and D. A. Mansfield, 1986: A study of wintertime circulation anomalies during past El Niño events using a high resolution general circulation model. Part I: Influence of model climatology. *Quart. J. Roy. Meteor. Soc.,* **112,** 613–638.

Pan, H.-L., and L. Mahrt, 1987: Interaction between soil hydrology and boundary layer developments. *Bound.-Layer Meteor.,* **38,** 185–202.

Rayner, N. A., E. B. Horton, D. E. Parker, C. K. Folland, and R. B. Hackett, 1996: Version 2.2 of the Global Sea-Ice and Sea Surface Temperature data set, 1903–1994. CERT No. 74, Hadley Center for Climate Prediction and Research, Bracknell, United Kingdom, 35 pp.

Reynolds, R. W., and T. M. Smith, 1994: Improved global sea surface temperature analyses using optimum interpolation. *J. Climate,* **7,** 929–948.

Ropelewski, C. F., and M. S. Halpert, 1987: Global and regional scale precipitation patterns associated with the El Niño/Southern Oscillation. *Mon. Wea. Rev.,* **115,** 1606–1626.

Schemm, J.-K., S. Schubert, J. Terry, S. Bloom, and Y. Sud, 1992: Estimates of monthly mean soil moisture for 1979–89, NASA Tech. Memo. 104571, Goddard Space Flight Center, Greenbelt, MD, 252 pp.

Schwarzkopf, M. D., and S. B. Fels, 1991: The simplified exchange method revisited: An accurate, rapid method for computation of infrared cooling rates and fluxes. *J. Geophys. Res.,* **96,** 9075–9096.

Shi, G. Y., 1981: An accurate calculation and the infrared transmission function of the atmospheric constituents. Ph.D. thesis, Dept. of Science, Tohoku University of Japan, 191 pp.

Shibata, K., and T. Aoki, 1989: An infrared radiative scheme for the numerical models of weather and climate. *J. Geophys. Res.,* **94,** 14 923–14 943.

Shukla, J., and M. J. Fennessy, 1988: Numerical simulation of the atmospheric response to the time-varying El Niño SST anomalies during May 1982 through October 1983. *J. Climate,* **1,** 195–211.

Simmons, A. J., J. M. Wallace, and G. W. Branstator, 1983: Barotropic wave propagation and instability, and atmospheric teleconnection patterns. *J. Atmos. Sci.,* **40,** 1363–1392.

Slingo, A., 1989: A GCM parameterization for the shortwave radiative properties of water clouds. *J. Atmos. Sci.,* **46,** 1419–1427.

——, and R. C. Wilderspin, 1986: Development of a revised longwave radiation scheme for an atmospheric general circulation model. *Quart. J. Roy. Meteor. Soc.,* **112,** 371–386.

Slingo, J. M., 1987: The development and verification of a cloud prediction model for the ECMWF model. *Quart. J. Roy. Meteor. Soc.,* **113,** 899–927.

——, and B. Ritter, 1985: Cloud prediction in the ECMWF model. ECMWF Tech. Rep. 46, European Center for Medium-Range Weather Forecasts, Reading, United Kingdom, 48 pp.

Smith, R. N. B., 1990: A scheme for predicting layer clouds and their water content in a general circulation model. *Quart. J. Roy. Meteor. Soc.,* **116,** 435–460.

Smith, R. N. B., 1993: Subsurface, surface and boundary layer processes. Met Office Unified Model Documentation Paper 24, 118 pp. [Available from NWP Division, UK Met Office, London Rd., Bracknell, Berkshire RG 12 2SZ, United Kingdom.]

Sud, Y. C., and G. K. Walker, 1992: A review of recent research on improvement of physical parameterizations in the GLA GCM. *Physical Processes in Atmospheric Models,* D. R. Sikka and S. S. Singh, Eds., Wiley Eastern, 422–479.

Tokioka, T., K. Yamazaki, I. Yagai, and A. Kitoh, 1984: A description of the Meteorological Research Institute atmospheric general circulation model (MRI GCM-I). MRI Tech. Rep. 13, Meteorological Research Institute, Ibaraki-ken, Japan, 249 pp.

——, ——, A. Kitoh, and T. Ose, 1988: The equatorial 30–60 day oscillation and the Arakawa–Schubert penetrative cumulus parameterization. *J. Meteor. Soc. Japan,* **66,** 883–901.

Trenberth, K. E., 1976: Spatial and temporal variations of the Southern Oscillation. *J. Roy. Meteor. Soc.,* **102,** 639–653.

——1997: The definition of El Niño. *Bull. Amer. Meteor. Soc.,* **78,** 2771–2777.

Volodin, E. M., and V. N. Lykossov, 1998: Parameterization of heat and moisture transfer in the soil–vegetation system for use in atmospheric general circulation models: 1. Formulation and simulations based on local observational data. (Translated from *Izvestiya AN.* Fizika Atmosfery i Okeana.). *Izv. Atmos. Oceanic Phys.,* **34,** 405–416.

Xie, P., and P. A. Arkin, 1997: Global preciptation: A 17–year monthly analysis based on gauge observation, satellite estimates, and numerical model outputs. *Bull. Amer. Meteor. Soc.,* **78,** 2539–2558.

Xue, Y. -K., P. J. Sellers, J. L. Kinter II, and J. Shukla, 1991: A simplified biosphere model for global climate studies. *J. Climate,* **4,** 345–364

Zang, G. J. and N. A. McFarlane, 1995: Sensitivity of climate simulations to the parameterization of cumulus convection in the Canadian Climate Centre general circulation model. *Atmos.–Ocean,* **33,** 407–446.